Revealing the Tectonic Structure of the Bay of Iskenderun Using the Markov Random Fields Method

Ali Muhittin ALBORA

Istanbul University-Cerrahpaşa, Faculty of Engineering
Department of Geophysical Engineering-Büyükçekmece Campus
E-mail: muhittin@iuc.edu.tr

ABSTRACT

One of the important issues in Gravity and Magnetic prospecting is to separate regional and residual anomalies. Determination of this separation between them is also crucial. Markov Random Fields (MRF) method is used to distinguish these anomalies. The most important property of this method is to make use of stochastic characteristic in neighborhood and 2D view. MRF does not need any training before use. This method is first applied to magnetic anomaly map consisting of prisms. After application, MRF method gives satisfactory results. We use Iskenderun Bay magnetic anomaly map to determined off-shore fault lines. According to our results, we reveal fault lines along Iskenderun Bay.

Keywords: Markov Random Fields (MRF); Iskenderun Bay; Fault Lines; Tectonic structure

INTRODUCTION

One of the most important effects in the interpretation of potentially sourced anomaly maps is to remove unwanted noise. In other words, the separation of near-surface (residual) and deep (regional) effects from each other is the most important problem in our studies. Another important factor in interpreting the maps of potential origin is the determination of discontinuity limits.

Therefore, in this study, Markov Random Fields (MRF) method, which is frequently used in filtering processes in electronics engineering, was applied to magnetic anomaly map from naturally sourced fields. In order to test the success of the method in synthetic fields, a model structure consisting of prismatic structures with different depths, coordinates, Inclination, Declination, and Susceptibility was used. Successful results were obtained in the model study from the MRF method. As the field application, the airborne magnetic anomaly obtained by Mineral Research and Exploration (MTA) of Iskenderun Bay was used. The most important feature of the MRF method is that it makes use of the stochastic structure of the two-dimensional image with neighborhood relations.

In addition, the MRF method does not require pre-training and therefore our data loss is reduced. Realized the first application of the MRF approach to two-dimensional images [1; 2; 3; 4]. As is known, Turkey is located on active tectonic therefore consists of a large number of influential earthquakes. In this study, the discontinuity boundaries of the aerial magnetic anomaly map of the Iskenderun region, which is a continuation of the Eastern Anatolian Fault (EAF) line, were determined by the MRF method and evaluated together with the seismic activity there. For this reason, the region has attracted the attention of many geologists and the tectonic discussions of the region still continue. In the GPS studies carried out in the region, information about the speed and directions of movement for 3 different plates in the region was given. [5; 6]. They followed the seismological movements of the major earthquakes that occurred in the region.

They examined the characteristics of the faults that dominate the region and the active tectonics of the region [7; 8; 9; 10; 11].

MARKOV RANDOM FIELDS METHOD (MRF)

In this study, the magnetic anomaly map is assumed to be a finite $N_1 \times N_2$ rectangular lattice of pixels defined as,

$$L = \left\{ (i,j) : 1 \le i \le N_1, 1 \le j \le N_2 \right\}.$$

Thus, the anomaly map can be considered as a matrix with $N_1 \times N_2$ pixels. A collection of subsets of L de

$$\eta = \left\{ \eta_{ij} : (i,j) \in L, \eta_{ij} \subseteq L \right\} \qquad (1)$$

is a neighborhood system on L if and only if η_{ij} the neighborhood of pixel (i,j) is such that, $(i,j) \notin \eta_{ij}$ if $(k,l) \in \eta_{ij}$ then $(i,j) \in \eta_{kl}$ for any $(i,j) \in L$. The cliques are the subgroups of the mth order neighborhood system, $\{ \eta^m \}$. A hierarchically ordered sequences of neighborhood systems that are commonly used in modeling are first and second neighborhood structures; $\{ \eta^1, \eta^2 \} = \{ \eta_{ij}^1, \eta_{ij}^2 \}$, respectively as in Figure 1 [2].

First neighborhood, $\eta^1 = \{ \eta_{ij}^l \}$ consists of the closest four neighbors of each pixel known as the nearest-neighbor model and is shown in Figure 1. Second neighborhood, $\eta^2 = \{ \eta_{ij}^2 \}$ consists of eight pixels neighboring (i,j) as in Figure 2. The cliques related with a lattice-neighborhood pair (L, η), denoted by c, is a subset of L such that scribed as, c consists of a single pixel,

or for $(i,j) \neq (k,l), (i,j) \in c$ and $(k,l) \in c$ implies that $(i,j) \in \eta_{kl}$.

The collection of all cliques of (L, η) is denoted by C = C (L, η). In some cases, only some of the cliques are more effective in the evaluation of a given pixel. Hence, these cliques can be selected as subgroups for a given neighborhood system. The cliques, except the single pixel clique, associated with η^2 are defined as,

We can rewrite expression (2) in terms of labeled pixels as,

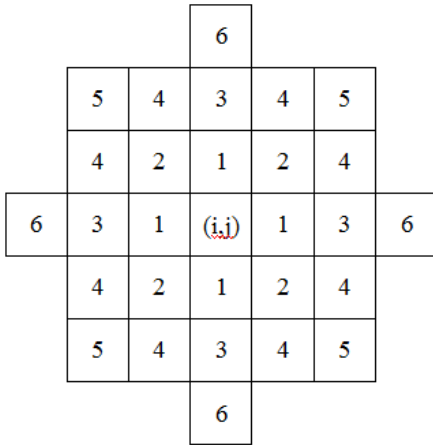**FIGURE 1:** Hierarchically arranged neighborhood system [2].

$$\begin{bmatrix} * & * \end{bmatrix}, \begin{bmatrix} * \\ * \end{bmatrix}, \begin{bmatrix} & * \\ * \end{bmatrix}, \begin{bmatrix} * \\ & * \end{bmatrix}, \begin{bmatrix} * & * \\ * \end{bmatrix},$$

$$\begin{bmatrix} * \\ * & * \end{bmatrix}, \begin{bmatrix} & * \\ * & * \end{bmatrix}, \begin{bmatrix} * & * \\ & * \end{bmatrix}, \begin{bmatrix} * & * \\ * & * \end{bmatrix}. \tag{2}$$

We can rewrite expression (2) in terms of labeled pixels as,

$$\begin{bmatrix} u_1 & u_2 \end{bmatrix}, \begin{bmatrix} v_1 \\ v_4 \end{bmatrix}, \begin{bmatrix} & v_2 \\ v_4 \end{bmatrix}, \begin{bmatrix} v_1 \\ & v_3 \end{bmatrix},$$

$$\begin{bmatrix} v_1 & v_2 \\ v_4 \end{bmatrix}, \begin{bmatrix} v_1 \\ v_4 & v_3 \end{bmatrix}, \begin{bmatrix} & v_2 \\ v_4 & v_3 \end{bmatrix}, \begin{bmatrix} v_1 & v_2 \\ & v_3 \end{bmatrix},$$

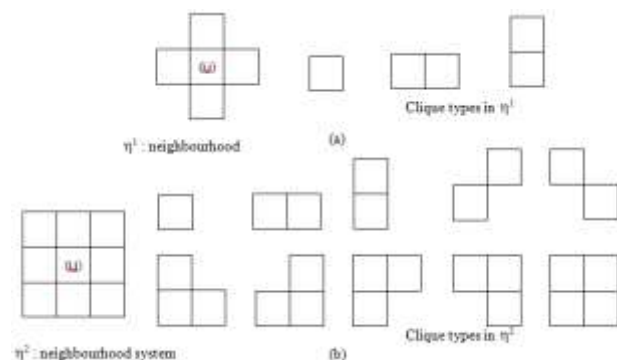$$\begin{bmatrix} v_1 & v_2 \\ v_4 & v_3 \end{bmatrix}. \tag{3}$$

FIGURE 2: Neighborhood systems η^1 and η^2 and their associated clique types.

In Expression (2), the first term viz., $\begin{bmatrix} * & * \end{bmatrix}$ means that the clique is composed of two pixels which are left and right neighbor of the original pixel. This clique includes pixels; $\{u_1, u_2\}$ as in the first term of Expression 3, $\begin{bmatrix} u_1 & u_2 \end{bmatrix}$. Similarly, the sixth term of (2), $\begin{bmatrix} * \\ * & * \end{bmatrix}$ is composed of 3 pixels; $\{v_1, v_3, v_4\}$ of $\begin{bmatrix} v_1 \\ v_4 & v_3 \end{bmatrix}$ clique of Expression (3). Again, the last term of Expression 2, viz., $\begin{bmatrix} * & * \\ * & * \end{bmatrix}$ means $\{v_1, v_2, v_3, v_4\}$ pixels are the elements of the clique, $\begin{bmatrix} v_1 & v_2 \\ v_4 & v_4 \end{bmatrix}$. The elements of all cliques with different neighborhood levels as shown in Figure 3, can be found easily in the same way [12].
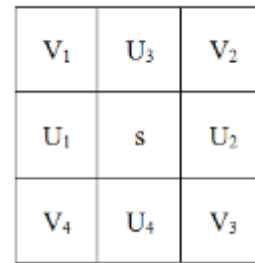

FIGURE 3: Neighborhood system of η^2. Here is observed pixel, $\{v_1, v_2, v_3, v_4\}$ are corner pixels and $\{u_1, u_2, u_3, u_4\}$ are left, right, up, down pixels [2].

Correct estimation and removal of the regional field from initial field observations yields the residual field produced by the target sources. Here, we wish to separate magnetic anomaly map Y= {Y $_{ij}$} and evaluate residual anomaly, X= {X $_{ij}$}. X is defined on L, has *Gibbs Distribution* (GD) or can be considered as equivalent to a *Gibbs Random Field (GRF)* with respect to η if and only if its joint distribution is of form,

$$P(X = x) = \frac{1}{Z} e^{-U(x)}, \tag{4}$$

where, $P(X = x)$ is the probability of residual anomaly map X, taking a specific quantization level value of x,

$U(x) = \sum_{c \in C} V_c(x)$, defined as *energy function,*

$V_c(x)$: potential associated with clique c and

$Z = \sum_s e^{-U(x)}$: Partition function, which is simply a normalizing constant.

So, the objective now is to have an estimation rule, that is, an algorithm, which will yield x* that maximizes the *a posteriori* distribution $P(X = x | Y = y)$ for a given y. Applying Bayes' rule, the *a posteriori* distribution can be written as,

$$P(X = x | Y = y) = \frac{P(Y = y | X = x)P(X = x)}{P(Y = y)}$$

(6)

Since probability $P(Y=y)$, does not effect maximization, $P(Y=y)$ can be ignored and the logarithm of Equation (6) can be written as [2],

$$\ln P(X = x, Y = y) = \ln P(X=x) + \ln P(Y = y | X = x) \quad (7)$$

We aim to optimize Equation 7. The two components of the joint log-likelihood in (7) can be expressed for MRF as,

$$\ln P(X = x) = -\ln Z - \sum_{c \in C} V_c(x) \quad (8)$$

$$\ln P(Y = y | X = x) = -\frac{N_1 N_2}{2} \ln(2\pi\sigma^2) - \sum_{m=1}^{M} \sum_{(i,j) \in S_m} \frac{1}{2\sigma^2}(s_{ij} - q_m)^2$$

(9)

where, $S_m = \{(i,j) \in L : X_{ij} = m\}$ and σ^2 is the variance of the noisy input image [12].

Let s represent (s_{ij}) which is the transient quantization level of the residual map during optimization at (i,j) pixel, defined in Equation (5) and t' be the vector of neighboring values of s,

$$t' = [u_1, u_2, u_3, u_4, v_1, v_2, v_3, v_4]^T \quad (10)$$

where, the location of u_i's and v_i's with respect to s are shown in Figure 3. We define indicator functions,

$$I(z_1, z_2, ..., z_k) = \begin{cases} -1 & , \quad z_1 \approx z_2 \\ 1 & , \quad \text{otherwise} \end{cases}$$

(11)

$\approx$ is expressed as,

$$z_k \approx z_{k+1} \text{ , if } |z_k - z_{k+1}| \leq \varepsilon \quad (12)$$

where ε is a positive real value used for approximation. Another indicator $J_m(s)$ is defined as,

$$J_m(s) = \begin{cases} -1. & , \quad s \approx q_m \\ 1 & , \quad \text{otherwise} \end{cases}$$

(13)

$\approx$ is expressed as,

$$s \approx q_m \text{ , if } |s - q_m| \leq \varepsilon \quad (14)$$

using indicators given in Equation (11) and (13). The potential function (8) of all cliques that contain (i,j), can be expressed the site of s as,

$$V(s, t', \theta) \equiv \sum_{c:q_m \in C} V_C(x) \quad (15)$$

where θ is the parameter vector to be found out. Thus both (8) and (9) are defined as a function of s, resulting common optimization. θ is defined as,

$$\theta = [\alpha_1, \alpha_2, .., \alpha_M, \beta_1, \beta_2, \beta_3, \beta_4, \gamma_1, \gamma_2, \gamma_3, \gamma_4, \xi_1]^T$$

(16)

where $\{\alpha_1, \alpha_2, .., \alpha_M\}$ parameter set gives the information about the similarity of the amplitude value of the evaluated pixel (s) and controls the percentage of pixels in each region type.

$\{\beta_1, \beta_2, \beta_3, \beta_4\}, \{\gamma_1, \gamma_2, \gamma_3, \gamma_4\}$ and ξ_1 parameters control the size and direction of separation.

Thus, optimum parameter values of Equation (16) will also result to an optimum quantization level set $\{q_1, q_2, .., q_M\}$ as the output of MRF process. $\{\alpha_1, \alpha_2, .., \alpha_M\}$ set is related with $\{J_1(s), J_2(s), .., J_M(s)\}$ as defined in Equation (13). To clarify the relationship between cliques in Expressions (2), (3) with more than one element and control parameters,

$$\{\beta_1, \beta_2, \beta_3, \beta_4, \gamma_1, \gamma_2, \gamma_3, \gamma_4, \xi_1\}$$

of θ vector, the below definitions can be done,

$$\begin{bmatrix} * & * \\ & \end{bmatrix}, \beta_1 \end{bmatrix}, \begin{bmatrix} * \\ * \end{bmatrix}, \beta_2 \end{bmatrix}, \begin{bmatrix} & * \\ * & \end{bmatrix}, \beta_3 \end{bmatrix}, \begin{bmatrix} * \\ * \end{bmatrix}, \beta_4 \end{bmatrix},$$

$$\begin{bmatrix} * & * \\ * & \end{bmatrix}, \gamma_1 \end{bmatrix}, \begin{bmatrix} * & \\ * & * \end{bmatrix}, \gamma_2 \end{bmatrix}, \begin{bmatrix} * & * \\ & * \end{bmatrix}, \gamma_3 \end{bmatrix}, \begin{bmatrix} & * \\ * & * \end{bmatrix}, \gamma_4 \end{bmatrix},$$

$$\begin{bmatrix} * & * \\ * & * \end{bmatrix}, \xi_1 \end{bmatrix}.$$

(17)

We can rewrite expression (17) in terms of labeled pixels as,

$$\begin{bmatrix} u_1 & u_2 \\ & \end{bmatrix}, \beta_1 \end{bmatrix}, \begin{bmatrix} v_1 \\ v_4 \end{bmatrix}, \beta_2 \end{bmatrix}, \begin{bmatrix} & v_2 \\ v_4 & \end{bmatrix}, \beta_3 \end{bmatrix},$$

$$\begin{bmatrix} v_1 \\ v_3 \end{bmatrix}, \beta_4 \end{bmatrix}, \begin{bmatrix} v_1 & v_2 \\ v_4 & \end{bmatrix}, \gamma_1 \end{bmatrix}, \begin{bmatrix} v_1 & \\ v_4 & v_3 \end{bmatrix}, \gamma_2 \end{bmatrix},$$

$$\begin{bmatrix} v_1 & v_2 \\ & v_3 \end{bmatrix}, \gamma_3 \end{bmatrix}, \begin{bmatrix} & v_2 \\ v_4 & v_3 \end{bmatrix}, \gamma_4 \end{bmatrix}, \begin{bmatrix} v_1 & v_2 \\ v_4 & v_3 \end{bmatrix}, \xi_1 \end{bmatrix}$$

(18)

The first term $\begin{bmatrix} * & * \\ & \end{bmatrix}, \beta_1 \end{bmatrix}$ of expression (17), shows the right adjacent pixel (u_1) and the left adjacent pixel (u_2) of the observed pixel (s). This case is also represented in the first term of expression (18), as $\begin{bmatrix} u_1 & u_2 \\ & \end{bmatrix}, \beta_1 \end{bmatrix}$. Here β_1 parameter shows the correlation between (u_1, u_2, s, q_m), where $\{u_1, u_2\}$ are adjacent pixels, (s) is observed pixel and (q_m) is quantized estimated value. In the second term, $\begin{bmatrix} * \\ * \end{bmatrix}, \beta_2 \end{bmatrix}$ of expression (16) and $\begin{bmatrix} v_1 \\ v_4 \end{bmatrix}, \beta_2 \end{bmatrix}$ of expression (18), β_2 parameter carries the information of the correlation of

(v_2, v_4, s, q_m). Other terms of expressions (17) and (18) can be easily evaluated in the same manner. Hence, control parameters of the control vector θ and their correlation between observed pixel, neighbor pixels, quantization levels are explained. Now, we can rewrite (15) as,

$$V(s,t',\theta) \equiv \phi^T(s,t')\theta. \qquad (19)$$

where,

$$\phi(s,t') = [J_1(s), J_2(s), ..., J_M(s), (I(s,u_1) + I(s,u_3)), (I(s,u_2) + I(s,u_4)),$$
$$(I(s,v_2) + I(s,v_4)), (I(s,v_1) + I(s,v_3)), (I(s,u_2,v_2) + I(s,u_4,u_3) + I(s,u_1v_4)),$$
$$(I(s,u_4,v_3) + I(s,u_2,u_3) + I(s,u_1,v_1)), (I(s,u_2,v_1) + I(s,u_1,u_4) + I(s,u_3,v_3)),$$
$$(I(s,u_1,u_2) + I(s,u_4,v_4) + I(s,u_3,v_2)), (I(s,u_1,v_1,u_2) + I(s,u_2,v_2,u_3) +$$
$$I(s,u_3,v_3,u_4) + I(s,u_4,v_4,u_1))]^T \qquad (20)$$

where *I,J* are indicators given by Equation (11) and (13). Suppose $P(s,t')$ is the joint distribution of random variables on 3x3 block centered at (i,j) and P (t') is the joint distributions on η_{ij} only [12].

APPLICATION OF MRF METHOD TO SYNTHETIC DATA
The MRF method has been used by many researchers in various application areas. The MRF method was first used as noise analysis [2]. They used the MRF method to determine the building boundaries [13; 14; 15]. They used the MRF method to locate the remains in archaeological sites [16; 17].

TABLE 1: Parameters of prisms of different sizes.

Parameters	Prism 1	Prism 2	Prism 3
X1; X2	15; 22	28; 34	18; 25
Y1; Y2	30; 35	10; 15	15; 27
Z1; Z2	5; 8	4; 6	8; 13
inclination	67	66	65
declination	0	5	4
Susceptibility	0.00194	0.00199	0.00204

As a synthetic study, 3 different prismatic structures with different sizes are considered. These prisms are in different coordinates and 2 prisms are close to the surface to create a residual effect, and the other prism is deeper to create a regional effect. Prisms have different inclination, equilibration and susceptibility values. The total magnetic anomaly map created by magnetic prisms with different parameters is shown in Figure 4. The MRF output given in Figure 4b was obtained by applying the MRF method to the total magnetic anomaly map (Figure 4a).
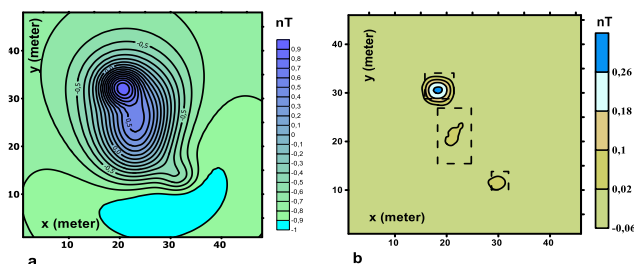

FIGURE 4: Prisms with different parameters a. Total magnetic anomaly map b. MRF output of the total magnetic anomaly map of the prisms (Dashed lines indicate possible locations of the prisms).

As another synthetic example, a total magnetic anomaly map of two perpendicular prisms is given (Figure 5a). Our aim in this synthetic study is to reveal the success of the MRF method in determining the structure boundaries. The MRF method has successfully determined the boundaries of two perpendicular prisms as seen in Figure 5b.
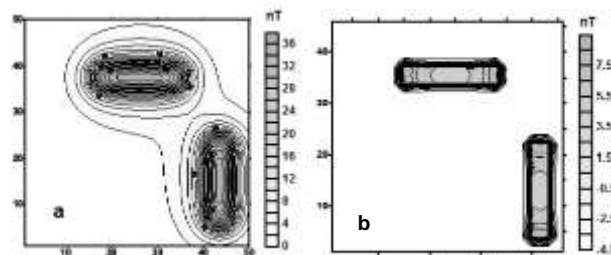

FIGURE 5: The synthetic model composed of two similar perpendicular prisms a) Vertical magnetic anomaly map (contour interval is 2 nT). b) MRF output (contour interval is 2 nT).

WORK AREA
Since the Study Area has a very complex structure, it has been studied with great interest by most researchers. The Eastern Anatolian Fault Zone (EAFZ) is a fault zone starting from Karlıova in the northeast and extending to Kahramanmaraş in the southwest (Figure 6).

This zone is a NE-SW trending, left-sided strike-slip fault. It joins with the North Anatolian Fault Zone in Karlıova and with the Dead Sea Fault Zone (ÖDFZ) around Türkoğlu in Kahramanmaraş and forms a triple joint here. The region has generally been under the influence of DAFZ and ÖDFZ. The effects of the three plates combined in this region.

Most researchers have conducted studies on the effect of DAFZ in this region (Figure 7). The EAF is a transform fault and compresses the Arabian-African and Anatolian-Eurasian plates with a lateral movement [8; 11; 18; 19; 20]. Different researchers have put forward different opinions on the continuation of the DAFZ after Maraş. Some of them claim that DAFZ extends to Antakya and merges with ÖDFZ here [21; 22; 23; 24]. A second view is that the DAFZ extends towards the Mediterranean or Cyprus. According to another view, the fault zone ends at the triple joint point. In this study, it was tried to shed light on the tectonic situation of the region by applying the MRF method to the map obtained by MTA, which has airborne magnetic anomaly in Iskenderun Bay.

The age of EAF has been estimated to be 4-5 (Pliocene) million years [23]. The total slip on this fault is 3.5-13 km. and 15-27 km considering the displacement of the pre-Pliocene units. has been proposed [18; 23].

FIGURE 6: Tectonic feature of the study area. They stated that the DAF has a displacement of 22 km and that the DAF has a shift rate of 4-7 mm / year [10]. He argued that most of the movement between Arabia and Anatolia was along the EAF [8]. They stated that the piece called the main

branch of the EAF starts from the triple joint near Karlıova and extends in the southwest direction to the south of Türkoğlu [21]. They revealed that the earthquake depths here are concentrated between 5-35 km.

When earthquake solutions are examined, it can be seen that the dominant faults in the region are strike-slip mechanisms with normal slip components (Figure 8). In some earthquakes occurring in the Adana region, they show full normal faulting characteristics [23; 26].
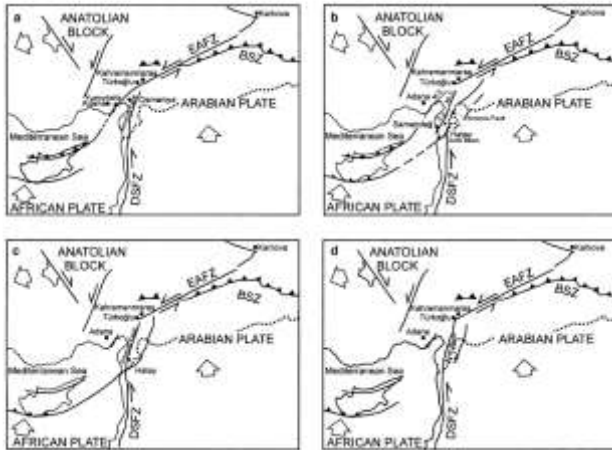

FIGURE 7: An alternative tectonic location map of the Eastern Anatolian Fault along the North Eastern Mediterranean is given. [8; 11; 18; 19; 20]. (b) Shortenings: M.S. Main ARM, Mi S: Middle branch and south branch of SS East Anatolian Fault [21]. (c) WSFZ: Ölüdeniz Fault Zone, EAFZ: East Anatolian Fault Zone [22; 23; 24]. Dotted lines indicate the Turkey-Syria border [25].
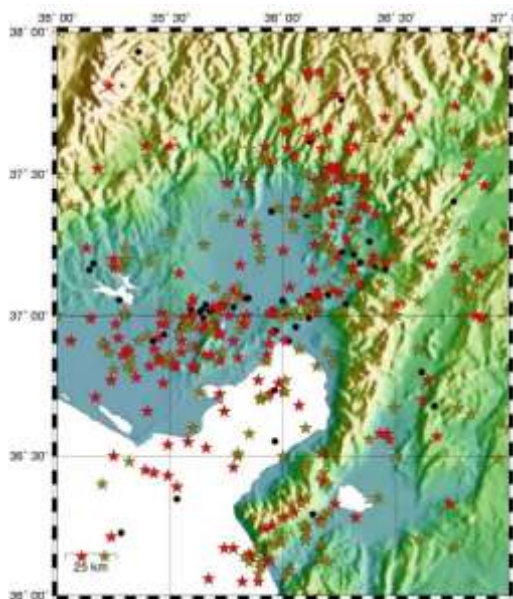

FIGURE 8: Earthquake activity of Iskenderun Bay and its surroundings (red stars, TÜBİTAK-MAM YDBAE catalog 1999 - 2001 Yellow stars show TÜBİTAK-MAM YDBAE catalog 1993 - 2001, dots show USGS catalog (1973-present)).

The solutions that dominate the region generally have left lateral strike-slip and normal-slip components. The region is in an earthquake-active place. Airborne magnetic anomaly map taken by Mineral Research and Exploration (MTA) in the region is given in Figure 9a. When the Airborne Magnetic anomaly map is examined, it is seen that values up to approximately 1500 nT have been measured in Iskenderun Bay. The mixed magnetic anomaly values in the Hatay region are thought to be caused by the

ophyalite structures in this region. It is known that ophyalite structures with magnetic properties surface here. At the same time, ophyalite structures, which also have magnetic properties, create a complex magnetic anomaly in the Hatay region. MRF method has been applied to the magnetic anomaly map and MRF output is shown in Figure 9b. As can be seen in the MRF output, we can say that there is an active fault line since there is a fault line that cuts through Iskenderun Bay and there are earthquakes occurring in this fault line and its branches.
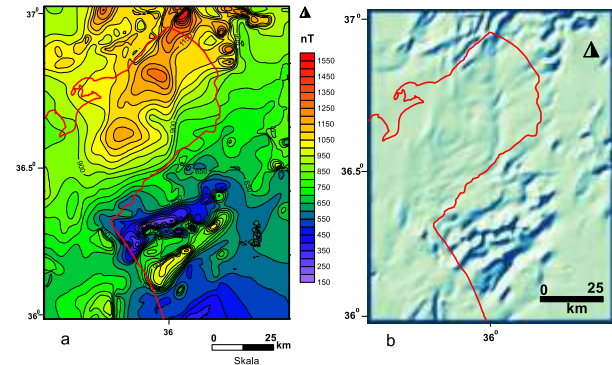

FIGURE 9: İskenderun Bay and its environs. a) airborne magnetic anomaly map (data from MTA) b) MRF printout.

RESULT

By applying the power spectrum method to the magnetic anomaly map obtained in Iskenderun Bay, they made depth maps [27; 28] in the Gulf of Iskenderun in Turkey sediment studies are conducted to assess the potential risks they create dangerous levels of pollution levels and environmental elements [29]. In this study, the success of the MRF method in border detection and regional residual separation was demonstrated in synthetic prisms. Then, MRF method was applied to the aerial magnetic anomaly map of Iskenderun Bay and is given in Figure 9b. Here, it was clearly revealed that there is a fault line in the north-south direction from the middle of the bay. Considering the earthquake activity of the region, it can be predicted that this fault line is an active fault and may produce earthquakes with magnitudes of 5 or more.

REFERANCE

[1] Geman, S., and Geman, D., "Stochastic Relaxation, Gibbs Distributions, and the Bayesian restoration of images", *IEEE PAMI*, 6:721-741, 1984.

[2] Derın, H., and Ellıot, A.H., "Modelling ans segmentation of noisy and textured images using Gibbs Random Field", *IEEE PAMI*, 9: 39-55, 1987.

[3] Dubes, R.C., and Jain, A., "Random field models in image analysis", *Journal of Applied Statistics*, 16:131-162, 1989.

[4] Uçan, O.N., Şen, B., Albora, A.M., and Özmen, A., "A New Gravity Anomaly Separation Approach: Differential Markov Random Field (DMRF)", *Electronic Geosciences*,5:1(1), 2000.

[5] Kahle, H-G., Straub, C, Reılınger, R., Mcclusky, S., Kıng, R., Hurst, K., Veıs, G., Kastens, K. And Cross, P., "The Strain Rate Field in The Eastern Mediterranean Region, Estimated by Repeated GPS Measurements", *Tectonohypsics,* 294: 237-252,199

[6] Kahle, H-G., Cocard, M., Peter, Y., Geiger, A., Reilinger, R., Barka, A. and Veis, G., "GPS-derived strain rate field within the boundary zones of the Eurasian, African and Arabian Plates", *J. Geophys. Res.,* 105: 23353-23370, 2000.

[7] Mckenzıe, D.P., "The Plate Tectonics Of The Mediterranean Region", *Nature,* 226: 239-241, 1970.

[8] Mckenzıe, D.P., "Active Tectonics of The Mediterranean Region", *Geophys. J. Astr. Soc,* 30(2): 109-185, 1972.

[9] Mckenzıe, D.P., "The East Anatolian Fault: A Majör Structure In Eastern Turkey, *Earth andp. Sci. Lett,* 29: 189-193, 1976.

[10] Dewey, J.F. and Şengör, A.M.C., "Aegean and surrounding regions: Complex multiplate and continuum tectonics in a convergent zone", *Geol. Soc. Am. Bull,* 90: 84-92, 1979.

[11] Taymaz, T., Eyıdoğan, H. and Jackson, J.A., "Source Parameters of Large Earthquakes in The East Anatolian Fault Zone", *Geophys. J. Int.,* 106: 537-550, 1991.

[12] Albora, A.M. and Uçan, O. N., "Separation of Magnetic Field Data Using Differential Markov Random Field (DMRF) Approach", *Geophysics,* 71: 125-134, 2006.

[13] Albora A.M., "Investigation of Tectonic Structure of Turkey-Hatay Region Using Markov Random Fields (MRF) ", *Journal of Scientific and Engineering Research,* 4: 86-93, 2017.

[14] Albora, A. M., Ucan, O. N., Aydoğan, A., "Modeling Potential Fields Sources In The Gelibolu Peninsula (Western Turkey) Using A Markov Random Field Approach", *Pure and Applied Geophysics*, 164: 1057-1080, 2007.

[15] Albora A.M., "Investigation of Fault Lines in İskenderun Gulf Using Markov Random Fields", 24nd IEEE Signal Processing and Communications Applications Conference (siu 2016), ZONGULDAK, TÜRKIYE, 16-19 Mayıs 2016, no.31, pp.1-4.

[16] Albora, A. M. ve Uçan, O. N. "Sivas-Kuşaklı bölgesindeki Hitit imparatorluğunun kalıntılarının araştırılması: Markov Random Filtre (MRF)" 13. Sinyal İşleme ve Uygulamaları Kurultayı SIU-Erciyes Ünv. Elektrik-Elektronik Müh. Böl. 16-18 Mayıs Kayseri, 2005.

[17] Uçan, O.N. and Albora, A. M. "Evaluation of Ruins of Hitit Empire in Sivas-Kusakli Region Using Markov Random Field (MRF)", *Near Surface Geophysics*, 7(2): 111-122, 2009.

[18] Hempton, M. R., "Constraints on Arabian plate motion and extensional history of the Red sea", *Tectonics*, 6: 687–705, 1987.

[19] Westaway, R. "Present-day kinematic of the Middle East and eastern Mediterranean", *J Geophys Res*, 99:12071–12090, 1994.

[20] Westaway, R, Arger, J., "The Gölbaşı Basin Southern Turkey: a complex discontinuity in a major strike-slip fault zone" *J Geol Soc (London),* 153: 729-744. 1996.

[21] Perinçek, D. and Çemen, I., "The structural relationship between the East Anatolian Fault and Dead Sea Fault Zones in Southern Turkey" *Tectonophysics,* 172: 331–340, 1990

[22] Yürür, M. T. and Chorowicz, J., "Recent volcanism, tectonics and plate kinematics near the junction of the African, Arabian and Anatolian plates in the eastern Mediterranean", *J Volcanol Geoth Res,* 85: 1–15, 1998.

[23] Arpat, E, and Şaroğlu, F. "East Anatolian Fault system; thoughts on its development", *Bull Geol Soc Turk*, 78: 33–39, 1972.

[24] Muehlberger, W. R. and Gordon, M. B. "Observations on the complexity of the East Anatolian Fault Turkey", *J Struct Geol* 9: 899–903, 1987.

[25] Albora, A. M., Sayın, N., Ucan, O. N. "Evaluation of Tectonic Structure of İskenderun Basin (Turkey) Using Steerable Filters" *Marine Geophysical Researches*, 27: 225-239, 2006.

[26] Alp, H. and Albora, A.M. "Tracing of East Anatolian Fault Zone by using Wavelet analysis method" e-*Journal of New World Sciences Academy*, (2),3: 232-240, 2007.

[27] Alp, H., Albora A.M. and Tur, H., "A View Of Tectonic Structure and Gravity Anomalies of Hatay Region Southern Turkey Using Wavelet Analysis", *Journal of Applied Geophysics*, 75:498-505, 2011.

[28] Demirel, S., "Evaluation of the geophysical data on Iskenderun Bay (in Turkish)" PhD Thesis, Istanbul Univ., Science Inst., Istanbul., 1993.

[29] Bilim, F. Aydemir, A. and Ateş A., "Tectonics and Thermal Structure iIn the Gulf of Iskenderun (Southern Turkey) From the Aeromagnetic, Borehole and Seismic Data" Geothermics 70, 206-221, 2017.